1 Introduction

Thermally-induced flow, commonly referred to as natural convection, encompasses two interpretations. Technically, *natural* convection denotes an intrinsic mechanism within a thermal system, in contrast to externally forced convection, to restore energy balance naturally. Conversely, from a macroscopic perspective, it embodies a governing mechanism in nature, impacting our planetary climate. More precisely, natural convection is a driving mechanism for weather patterns. Furthermore, the crust of our home planet is in motion, driven by the same phenomena in the Earth's mantle.

The interplay between Earth's gravity and fluid density disparities has been extensively studied across diverse environments. Relationships between fluid properties and heat application have been well-explored under constant gravitational acceleration. However, Thermo-Electro Hydrodynamics (TEHD) introduces a novel dimension by allowing force fields in various geometric boundary conditions and a variable buoyancy acceleration. The result is a convective system wherein an electric field can actively control the strength and direction of heat flux. This capacity for controlling the buoyancy acceleration broadens the potential applications of TEHD. One geophysically relevant application involves establishing a radial force field within curved experimental geometries. For these experiments, a microgravity environment is appreciated to separate the effects of terrestrial gravity and TEHD.

Experimentally investigating flows under microgravity conditions has a long tradition in Cottbus. A project of particular importance is GeoFlow with its two spherical shell experiments, modelling Earth's mantle and designated to operate on the Iternational Space Station (ISS). The second GeoFlow mission, GeoFlow II, commenced in March 2011 and in-

cluded several modifications to its predecessor, GeoFlow I. Fundamental changes included the implementation of an outer cooling loop, a shift in the working fluid, and an increase in the operative Rayleigh number. The silicone oil was substituted by the fatty alcohol, 1-Nonanol, to utilise a fluid with temperature-dependent viscosity to simulate mantle convection more accurately. However, this change inadvertently introduced a significant internal heating effect.
Initially, this internal heating was not considered when Futterer et al. (2013) compared the first results from the GeoFlow II mission with numerical investigations. As a result, Futterer et al. noticed a mismatch between numerical and experimental flow patterns. With the introduction of Open Source Field Operation and Manipulation (OpenFOAM) software for TEHD simulations by the master thesis of Haun (2017), the dielectric heating effect was introduced. Numerical investigations of the GeoFlow IIc experiment, including the internal heating, showed a more conceivable match to interferometry images than before. The presented thesis aims to expand and verify the investigation done in the master thesis (Haun, 2017) and to build the theoretical baseline for TEHD with fluids affected by internal heating.

The primary focus of this work revolves around analysing and comprehending the GeoFlow experimental data using numerical investigations. This approach is extended through studies conducted in simplified 2D geometries to gain a deeper understanding. Moreover, the findings are utilised to plan and classify the subsequent space experiment, AtmoFlow. This thesis follows the frame of Introduction Methods Results and Discussion (IMRaD), emphasised by the *Publication Manual of the American Psychological Association, 7th Ed* (2020) and Glasman-Deal (n.d.).

1.1 Problem statement: The GeoFlow and AtmoFlow experiments

This chapter introduces two microgravity experiments as applications for TEHD to set the framework for this study and outlines the relevant associated features. The GeoFlow project comprises three spherical shell experiment campaigns aimed at geophysical flows, while AtmoFlow, its successor, focuses on atmospherical flows. Both GeoFlow and AtmoFlow experiments are designed for operation under microgravity conditions. Chapter 1.2 provides a chronological overview of the history and outcomes of the GeoFlow campaigns. However, this study only investigates the latest campaign's results of GeoFlow IIc.

Figure 1.1(a) and (b) show photos of both experiments, and below the photos are the cross-sections of the Computer Aided Design (CAD) model displayed in Figure. 1.1(c,d). They provide a detailed insight into the experiment designs. The GeoFlow experiment consists of an *inner sphere* (see Fig. 1.1(c)) made of steel with a radius of $R_1 = 0.0135$m. This sphere is mounted on a shaft. The shaft holds the inner sphere in position and provides a water circuit to thermalise the inner sphere (*heating circuit*) to a constant temperature T_h. The second layer is the outer shell, made of glass; it has an upper and lower half, flanged at the equatorial zone. The inner radius of this *outer shell* is the outer radius of the fluid gap $R_2 = 0.027$m. The region of interest is the gap filled with a dielectric fluid between the inner sphere and the glass shells ($d = R_2 - R_1$). There is an additional small gap, followed by another glass shell. This gap serves as a *cooling circuit*, ensuring the glass shell maintains a constant temperature of T_c.

On the right-hand side of Figure 1.1(b,c), the AtmoFlow experiment is shown. In contrast to GeoFlow, the inner sphere assembly consists of multiple parts and materials. The heating circuit is channelled in a torus-shaped cut-out inside the *inner sphere* near the equator. This circuit is thermally insulated to the steel sphere in the North and South Pole directions. The insulating material is Polyether Ether Ketone (PEEK), coloured light brown in Figure 1.1(d). The outer radius of

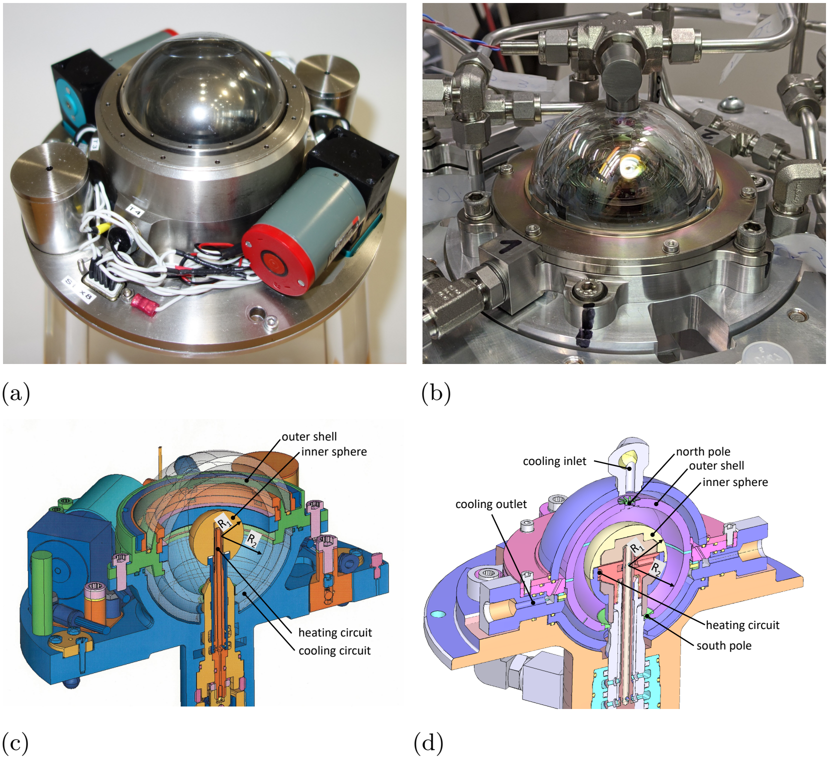

Figure 1.1: Photo of GeoFlow science reference model (a), and AtmoFlow breadboard experiment (b) and their corresponding Computer Aided Design (CAD) model cross-sections below (c,d). Some parts are marked for better orientation. The investigated domain is the spherical gap between the inner sphere (R_1) and outer shell (R_2).

the inner steel sphere is $R_1 = 0.0189$m, thus larger than the GeoFlow equivalent. The shaft radius is also wider because of the integration of a rotation feature that allows the inner sphere to rotate independently from the outer glass shells. The bearings seen in the lower part of the cross-section in Figure 1.1(d) indicate the rotation feature. However, this feature has not been investigated in this study.
Then, the fluid gap is enclosed by the *outer shell* of glass with a radius of $R_2 = 0.027$m. Thus, the outer dimension is the same as in GeoFlow, but the aspect ratio increased from $\eta = 0.5$ to 0.7. At the poles of this glass shell are two inserts made of copper, coloured in green in Figure 1.1(c). The upper insert defines the North Pole, and a ring insert between the shaft and the outer glass shell defines the South Pole. These inserts should provide a higher heat flux and lower temperature in these areas than in the glass shell. A cooling circuit encloses the outer shell, with the cooling circuit inlet directly above the copper insert. With emphasised heat flux in equatorial and pole regions, this construction shall model atmospheric-like temperature boundary conditions.

The numerical model's geometric and thermal boundary conditions are derived from the cross sections. The GeoFlow model is approximated as a spherical gap geometry with a fixed temperature at the inner and outer shell ($T_h > T_c$ with $T_h = T(R_1)$ and $T_c = T(R_2)$). In contrast, the AtmoFlow numerical model should address the different heat fluxes due to inhomogeneous material compositions at the boundary shells.

Moreover, the primary features of the experiments cannot be displayed in a CAD cross-section, which are an electric conductive coating of the inner surface of the glass shell and the high voltage supply. Thus, an electric field is established in the fluid gap, inducing a buoyancy force. In contrast to the terrestrial buoyancy force, this electric force is controllable in the experiment environment. The strength of the electric force is adjustable within the limits of applicable voltage. Furthermore, the boundary conditions define its direction; this opens opportunities to create a radial force field in spherical shell geometry similar to planets' gravitational force.

In the case of GeoFlow, the analogy to mantle convection, and for AtmoFlow, large-scale weather phenomena are in the scope of investigations. Hence, these flow structures discussed in this thesis cannot be observed in laboratory experiments due to the dominance of terrestrial gravity over the radial electric force. These experiments require microgravity conditions to insulate the electrical buoyancy effects and establish a purely radial force field, which can be achieved in long-term environments such as space stations. The utilised electric buoyancy force is the dielectrophoretic force acting on a dielectric fluid in a high voltage, high frequency (10kHz) Alternating Current (AC) electric field. Even so, this also resamples the working principle of microwave ovens. That means there is also expected to be a volumetric heating effect for various fluids under these operating conditions. The volumetric heating effect caused by the electric field is called dielectric heating. A more detailed description will follow in Section 2.1. In the case of the GeoFlow experiment, this effect was not addressed in the planning phase. Nevertheless, a posteriori, internal heating is a welcomed feature because it fits the analogy of volumetric heating in the Earth's mantle due to radiative decay.

The trade-off to the geometric similarity to planets is the accessibility to measurement methods. Using particle-based visualisation methods such as Particle Image Velocimetry (PIV) for long-duration space experiments is impracticable. Since the whole experiment is usually locked into a container, the operation and maintenance effort for the astronauts should be as low as possible. In particle-based methods, the particles in experiments possibly cause abrasion due to collision with each other or the experiment's infrastructure and tend to agglomerate over time. Furthermore, the interaction between particles and the electric field would require extensive investigations. Another complication for optical measurement techniques is the spherical geometry because many established optical methods rely on a beam going through the experiment. In the case of GeoFlow and AtmoFlow, the beam must reflect at the inner sphere in a spherical shell geometry. Therefore, the Wollaston Shearing Interferometry (WSI) was chosen as the optical measurement method for both experiments. For the GeoFlow missions, the optical periphery for WSI was provided by the Fluid Science Laboratory (FSL). Therefore, an external device was attached to the front panel of the experiment container. In contrast, AtmoFlow's optical system of WSI is included in the experiment container. It features two polarisation directions simultaneously instead of sequential as in GeoFlow (see Section 2.6.2). Thus, this is a new development that shall overcome the limitations of GeoFlow's optical system. Figure 1.1(a) shows the engineering model of GeoFlow, which was built to verify the engineering design; it shall be fully functional. Whereas the periphery of the Columbus Orbital Facility (COF), FSL is missing. The displayed model was neither meant to go to ISS nor verify the optical system since the interferometry apparatus was outsourced to the FSL. In contrast, the AtmoFlow thermal breadboard experiment (Figure 1.1(b)) was built to verify the thermal and optical path concepts. However, the photo and CAD model show only the experiment; the optical system components are not in the photos.

The WSI assembly contains a laser, several mirrors, lenses, polarisers and two Wollaston prisms. In the GeoFlow experiments, the lenses which focus the laser beam on the inner sphere define the field of view. In contrast to AtmoFlow, there was no co-rotating with the spherical shell assembly. Moreover, to scan the whole hemisphere with the field of view, the spherical shell assembly have constantly been rotating with the low rotation speed of 0.008Hz, even in the cases defined as "non-rotating". For the numerical investigation, this rotation was neglected. A detailed description of the WSI, explaining what is observed in the interferometry images, is provided in the post-processing Section 2.6.2.

The fundamental properties of both experiments are summarised in Table 1.1. Hence, temperature-dependent viscosity is of interest for geophysical applications; that is why the 1-Nonanol fluid was chosen for the GeoFlow II experiment to evolve a decisive viscosity difference between the inner and outer shell. Furthermore, two base temperatures T_c are applied. Temperature-dependent viscosity is not applied to numerical investigations in this study since the impact on the flow structure was not as decisive as expected. Nevertheless, the effect of different base temperatures on the Prandtl number is considered.

Property	Symbol	GeoFlow II	AtmoFlow
Fluid name		1-Nonanol	Novec 7200
Chemical formula		$C_9H_{20}O$	$C_4F_9OC_2H_5$
Inner radius	R_1	0.0135m	0.0189m
Outer radius	R_2	0.027m	0.027m
Maximum effective voltage	V_{rms}	4596V	5000V
Maximum temperature difference	ΔT_B	9.5K	20K
Prandtl number	Pr	125, 175	10

Table 1.1: Key properties of both space experiments, see Tab. 2.4 for all utilised fluid properties.

In conclusion, GeoFlow and AtmoFlow are spherical shell experiments utilising TEHD under microgravity conditions. In contrast, they are planned to operate with two aspect ratios and three Prandtl numbers. Additionally, AtmoFlow has non-uniform temperature boundary conditions, and the applied temperature difference is considerably significant with 20K, plus additional heat from the dielectric heating effect.

1.2 State of the art

TEHD can be classified as a sub-category of thermal convective flow. Since this study aims to derive the fundamentals of the GeoFlow experiment, the complexity of this experiment requires a broad knowledge due to the multiple flow aspects condensed in it. This section briefly overviews the main hypotheses and theories used in the relevant disciplines. It is organised by the topics, beginning with geophysically relevant investigations, continuing with TEHD investigations and ending with TEHD numerical and experimental investigations specific to GeoFlow; each subsection presents the literature chronologically. The selection of presented literature is based on their influence on the thesis's author; it shall make the chosen preferred methods and investigated properties clear for the reader.

1.2.1 Geophysical investigations

The GeoFlow experiment asserts its geophysical relevance due to its spherical structure and the establishment of a radial force field. Consequently, publications in geophysics-focused journals hold particular significance. The relevant research can be categorised into two areas: firstly, the combination of boundary-applied temperature difference and internal heating, called *mixed heating* convection (naming followed Vilella and Deschamps (2018)), holds relevance in modelling mantle convection. Secondly, several research studies focus on progressing from planar geometries to curved configurations such as infinite-length cylindrical annuli or slices of spherical shells. In both topics, the derivation of scaling laws is of particular interest as the results must be scalable for application to real planets. Furthermore, computational constraints made two-dimensional computational domains more prevalent in geophysics until the mid-1970s.

F. H. Busse (1975) set a landmark in flow pattern investigation; F. H. Busse mathematically predicted the formation of various patterns in spherical shell convection with radial buoyancy forcing. Later, Zebib, Schubert, Dein and Paliwal (1983) investigated the onset of convection in spherical shell geometry with varying aspect ratios. They formulated the critical Rayleigh numbers and investigated the heat flux, represented by the Nusselt number, and the "plan forms" (flow patterns) for boundary and internal heated configurations.

The Rayleigh number is named after Rayleigh (1916) and describes the strength of buoyancy-driven flow. It is defined as:

$$\mathrm{Ra} = \frac{\beta \Delta T g d^3}{\nu \kappa_T}, \tag{1.1}$$

with β as thermal expansion coefficient, ΔT as temperature difference, g as gravitational acceleration, d as characteristic length, ν as kinematic viscosity and κ_T as thermal diffusivity. Moreover, the critical Rayleigh number describes the tipping point when buoyancy forcing is strong enough to trigger thermal convection.

In 1989, Bercovici et al. conducted several 3D simulations of spherical shell convection using two distinct codes employing spectral methods. They reached a Rayleigh number approximately 100 times the critical Rayleigh number and could refine the predictions of F. H. Busse (1975). Using an infinite Prandtl number and a free slip boundary model, they identified stable tetrahedral and cubic convective patterns at the same Rayleigh number. All their simulations converged to stationary solutions.

Travis, Olson and Schubert (1990) conducted another significant study focusing on investigating the Nusselt number scaling for Rayleigh numbers ranging from 10^3 to 5×10^5 in 3D-planar geometry. They found the transition to 3D flow patterns between $\mathrm{Ra} \in [4 \times 10^4, 5 \times 10^5]$ and to in-stationarity at $\mathrm{Ra} \in [10^6, 10^7]$.